analytical chemistry

pubs.acs.org/ac Letter

Cryogenic Infrared Spectroscopy Reveals Structural Modularity in the Vibrational Fingerprints of Heparan Sulfate Diastereomers

Maike Lettow,[§] Márkó Grabarics,[§] Kim Greis, Eike Mucha, Daniel A. Thomas, Pradeep Chopra, Geert-Jan Boons, Richard Karlsson, Jeremy E. Turnbull, Gerard Meijer, Rebecca L. Miller, Gert von Helden, and Kevin Pagel*

Cite This: *Anal. Chem.* 2020, 92, 10228−10232 Read Online

ACCESS | Metrics & More | Article Recommendations | Supporting Information

ABSTRACT: Heparan sulfate and heparin are highly acidic polysaccharides with a linear sequence, consisting of alternating glucosamine and hexuronic acid building blocks. The identity of hexuronic acid units shows a variability along their sequence, as D-glucuronic acid and its C5 epimer, L-iduronic acid, can both occur. The resulting backbone diversity represents a major challenge for an unambiguous structural assignment by mass spectrometry-based techniques. Here, we employ cryogenic infrared spectroscopy on mass-selected ions to overcome this challenge and distinguish isomeric heparan sulfate tetrasaccharides that differ only in the configuration of their hexuronic acid building blocks. High-resolution infrared spectra of a systematic set of synthetic heparan sulfate stereoisomers were recorded in the fingerprint region from 1000 to 1800 cm^{-1}. The experiments reveal a characteristic combination of spectral features for each of the four diastereomers studied and imply structural modularity in the vibrational fingerprints. Strong spectrum-structure correlations were found and rationalized by state-of-the-art quantum chemical calculations. The findings demonstrate the potential of cryogenic infrared spectroscopy to extend the mass spectrometry-based toolkit for the sequencing of heparan sulfate and structurally related biomolecules.

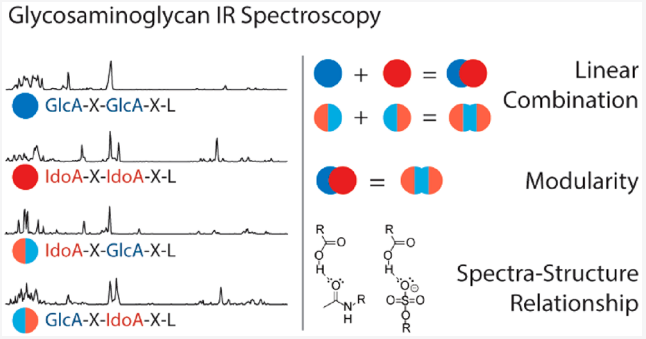

Heparan sulfate and heparin are structurally closely related, sulfated representatives of glycosaminoglycans (GAGs), a class of acidic polysaccharides with a linear sequence of repeating disaccharide units.[1,2] Being present in the extracellular matrix and at the surface of cells, they regulate various biological processes, ranging from hemostasis to inflammation and tumor metastasis.[3−5] The backbone of heparan sulfate and heparin consists of alternating α-D-glucosamine (GlcN, often acetylated as GlcNAc) and hexuronic acid building blocks. The identity of the hexuronic acid units varies in heparan sulfate and heparin chains: β-D-glucuronic acid (GlcA) and its C5 epimer, α-L-iduronic acid (IdoA), are both present. This backbone diversity is unique among GAGs and represents a major challenge for structural characterization.

Recent developments in electron-based ion dissociation methods enabled tandem mass spectrometry to overcome many difficulties in GAG analysis stemming from the presence of multiple sulfate groups[6−9] and from the potential variability of hexuronic acid stereochemistry.[10−12] Despite these improvements, an unambiguous distinction between GlcA and IdoA in isomeric heparan sulfate sequences is still extremely challenging and, in certain cases, may prove to be impossible by mass spectrometry alone.[13]

A promising strategy to unravel hexuronic acid stereochemistry is to employ ion mobility-mass spectrometry (IM-MS). IM-MS has been successfully applied for the analysis of intact GAG ions[14−16] as well as of their fragments to facilitate the sequencing of larger structures in a bottom-up approach.[17] Besides improving the speed and confidence of analyte identification, IM-MS often enables the separation and differentiation of heparan sulfate ions that differ only in the stereochemistry of hexuronic acid building blocks. In certain cases, however, the mobilities of such diastereomers are too similar, impeding an unambiguous structural assignment by IM-MS.

Previous studies revealed that mass-selected GAG ions exhibit characteristic spectral features in the mid-infrared[18,19]

Received: May 12, 2020
Accepted: July 13, 2020
Published: July 13, 2020

https://dx.doi.org/10.1021/acs.analchem.0c02048
Anal. Chem. 2020, 92, 10228−10232

and OH-stretching region.[20−22] Cryogenic temperatures in either messenger-tagging infrared (IR) spectroscopy[20] or helium nanodroplet IR spectroscopy[18] are crucial in the identification of GAG ions larger than monosaccharides. Both cryogenic IR spectroscopy approaches yield spectra that are reproducible and comparable across laboratories and instruments.[23] Building on these findings, we here employ cryogenic IR spectroscopy in helium nanodroplets to study the influence of hexuronic acid stereochemistry on the vibrational fingerprints of heparan sulfate oligosaccharide ions from 1000 to 1800 cm^{-1}.

The utilized experimental setup is shown in Figure 1 and has been described in detail previously.[24,25] In the present study, negative ions are generated by nanoelectrospray ionization (nESI), transferred to vacuum, and isolated using a quadrupole mass filter. The m/z-selected anions are directed into a cryogenic hexapole ion trap (90 K) where they undergo buffer-gas cooling. Subsequently, a stream of superfluid helium nanodroplets traverse the trap to pick-up the anions, which rapidly cool to 0.4 K, the equilibrium temperature of the droplets. The He-embedded anions overcome the trapping potential and reach the interaction region, where they are irradiated with intense, tunable radiation from the Fritz Haber Institute free-electron laser (FHI FEL). Upon sequential resonant absorption of multiple photons, the ions are released from the droplets and detected in a time-of-flight mass analyzer. IR action spectra are generated by plotting the ion signal as a function of the incident photon energy.

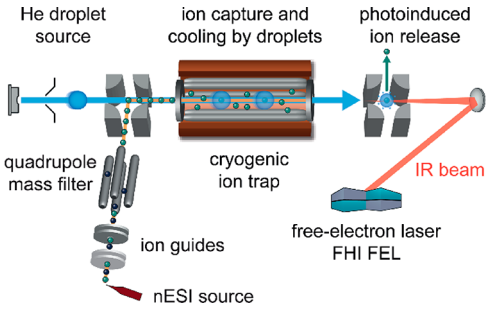

Figure 1. Schematic depiction of the helium nanodroplet instrument for cryogenic IR spectroscopy. Ions generated by nanoelectrospray ionization (nESI) are m/z-selected in a quadrupole and accumulated in a cryogenic ion trap at 90 K. Here, the ions are picked up by traversing superfluid helium nanodroplets and cooled to their equilibrium temperature of 0.4 K. Helium droplet-embedded ions are irradiated by IR photons coming from the Fritz Haber Institute free-electron laser (FHI FEL). Upon resonant absorption of multiple infrared (IR) photons, ions are released from the nanodroplets and detected after time-of-flight analysis. Plotting the ion release yield as a function of photon energy results in high-resolution vibrational spectra of cold, mass-selected ions.

For the experiments, a set of well-defined, aminoalkyl-linked synthetic heparan sulfate tetrasaccharides were chosen. The four tetrasaccharides represent a complete set of all possible permutations with repetitions of GlcA and IdoA; the rest of the molecule is identical.[26] The chemical structures are shown in Figure 2 and in Figure S1 (Supporting Information) in their representation using the symbol nomenclature for glycans (SNFG). In the four tetrasaccharides, the configurations at two stereogenic C5 atoms are varied, which makes them diastereomers and in pairs of epimers with only one alteration. These moderately sulfated tetrasaccharides were investigated as doubly deprotonated ions $[\text{molecule} - 2\text{H}]^{2-}$ with m/z 510, which makes them relatively stable in the gas-phase environment of a mass spectrometer.[18] The tetrasaccharides carry two 6O-sulfate functional groups (6S) at which the charges are localized.[19] Thus, charge migration and population of multiple deprotomers can be limited which decreases the spectral complexity.[18,27]

Cryogenic IR spectra in the fingerprint mid-IR range from 1000 to 1800 cm^{-1} were recorded and are shown in Figure 2. All spectra consist of well-resolved lines, and the four diastereomers can be unambiguously distinguished from each

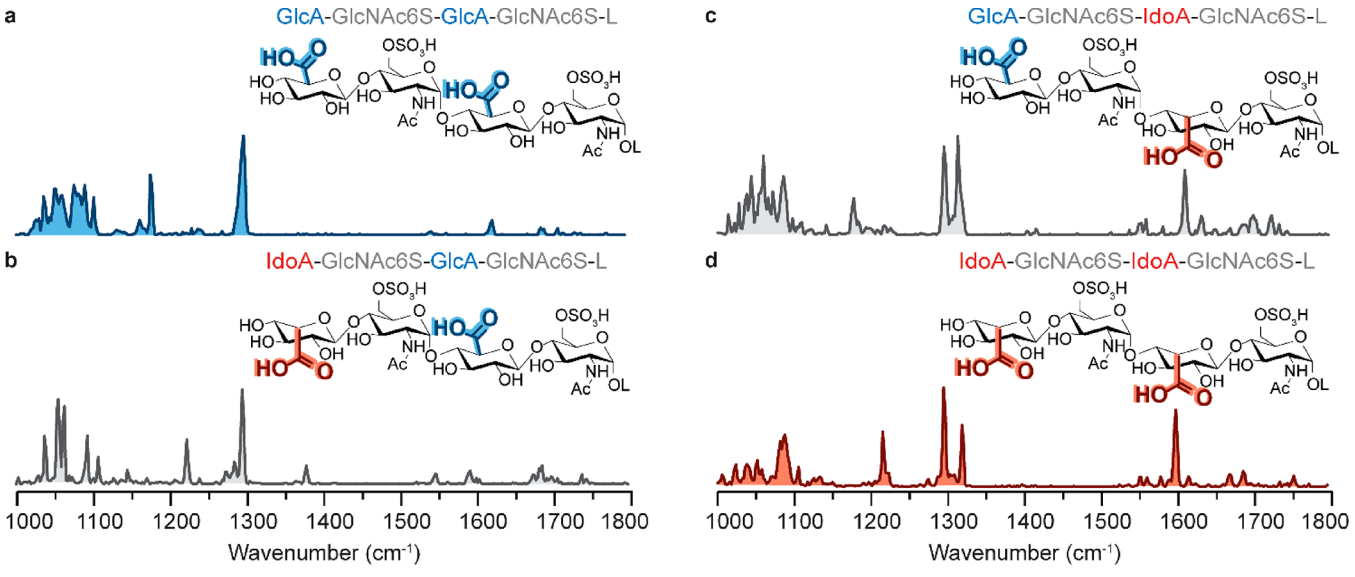

Figure 2. Cryogenic IR spectroscopy in helium nanodroplets from 1000 to 1800 cm^{-1} of heparan sulfate tetrasaccharides: (a) GlcA-GlcNAc6S-GlcA-GlcNAc6S-L, (b) IdoA-GlcNAc6S-GlcA-GlcNAc6S-L, (c) GlcA-GlcNAc6S-IdoA-GlcNAc6S-L, (d) IdoA-GlcNAc6S-IdoA-GlcNAc6S-L, investigated as $[\text{molecule} - 2\text{H}]^{2-}$ anions with m/z 510. Abbreviated are β-D-glucuronic acid GlcA, α-L-iduronic acid IdoA, 6-O-sulfo-N-acetyl-α-D-glucosamine GlcNAc6S, and aminoalkyl-linker L ($(CH_2)_5NH_2$) from synthesis.

https://dx.doi.org/10.1021/acs.analchem.0c02048
Anal. Chem. 2020, 92, 10228−10232

other based on their IR signatures. Assignments of spectral lines within wavenumber ranges are based on theoretical calculations of disaccharides (Figure S2, Supporting Information) and previously published calculations of sulfated monosaccharides.[19] For all four anions, the spectral features observed from 1000 to 1150 cm^{-1} can be assigned to combined C−O and C−C stretching vibrations of the glycan core. Additionally, the symmetric SO_3^- stretching modes of the sulfate functional groups are typically found around or below 1050 cm^{-1} and usually overlap. Spectral lines corresponding to the combined, antisymmetric SO_3^- stretching modes are observed between 1150 and 1350 cm^{-1}. Smaller features from 1200 to 1500 cm^{-1} correspond to multiple C−H and O−H bending modes. For the GlcNAc moieties, the amide I and II vibrations, the stretching vibration of the C═O and the combined bending modes of the N−H, respectively, are expected to be active between 1500 and 1700 cm^{-1}. Above 1700 cm^{-1}, spectral lines correspond to the C═O stretching vibration in the neutral carboxyl functional groups of GlcA and IdoA.

The region between 1000 and 1150 cm^{-1} in the spectra in Figure 2 is congested for all four species. At higher wavenumbers, however, characteristic bands can be observed, allowing for specific assignments. In the spectra in Figure 2a,c, a band at around 1175 cm^{-1} is observed. In the spectra in Figure 2b,d, this band seems to be replaced by a band at ∼1220 cm^{-1}. It is thus reasonable to assign the band at 1175 cm^{-1} to stem from the sulfate group in GlcA-GlcNAc6S and the band at ∼1220 cm^{-1} from the sulfate group in IdoA-GlcNAc6S, both at the nonreducing end. Moving to higher wavenumbers, in all four spectra, a band is observed at 1295 cm^{-1}. To the higher wavenumber side in the spectra in Figure 2c,d, a band at 1330 cm^{-1} is observed, which appears to be connected to the presence of the sulfate group in IdoA-GlcNAc6S-L at the reducing end of the glycan. At higher wavenumbers around 1600 cm^{-1}, an intense band is observed in the spectra in Figure 2c,d, which again coincides with the disaccharide IdoA-GlcNAc6S-L at the reducing end. The absorption bands in the region of the antisymmetric SO_3^- stretching modes are always present in two IR spectra, in an IR spectrum of a homogeneous diastereomer (either two GlcA or two IdoA) and in an IR spectrum of a heterogeneous diastereomer (one GlcA and one IdoA), with the exception of the vibration at 1295 cm^{-1}.

The difference in the absorption pattern in the region of the antisymmetric SO_3^- stretching region likely reflects a hexuronic acid-dependent change in the chemical environment of the sulfate groups. With the variation in the hexuronic acid stereochemistry, the hydrogen-bonding network in the tetrasaccharides seems to change. Furthermore, the local conformation in the disaccharide modules appears discrete, i.e., without strong hydrogen-bonding networks to the rest of the chain.

To test whether the absorptions derive from chemically discrete modules of disaccharides in the tetrasaccharide, the linear combinations of the IR spectra of the homogeneous diastereomers and of the IR spectra of the heterogeneous diastereomers were constructed and are shown in Figure 3a. Assuming discrete increments of disaccharides with discrete IR signatures, both linear combinations represent a 1:1:1:1 combination of the IR signatures of all possible disaccharide modules, GlcA-GlcNAc6S, IdoA-GlcNAc6S, GlcA-GlcNAc6S-L, IdoA-GlcNAc6S-L, at the nonreducing end or at the

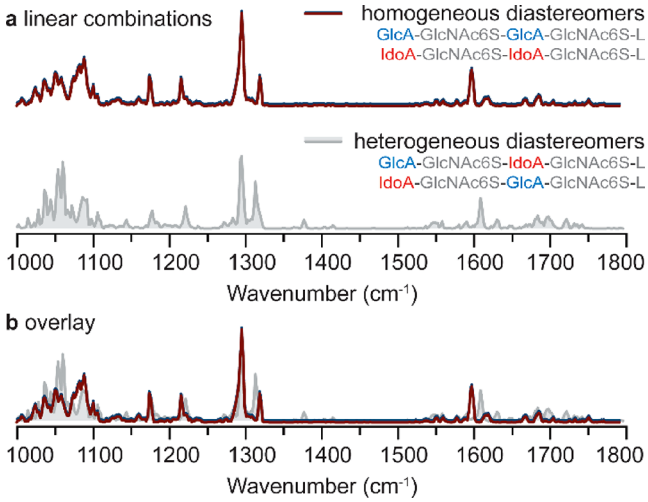

Figure 3. (a) Linear combinations of the cryogenic IR spectra in helium nanodroplets from 1000 to 1800 cm^{-1} of the homogeneous diastereomers (upper panel) GlcA-GlcNAc6S-GlcA-GlcNAc6S-L and IdoA-GlcNAc6S-IdoA-GlcNAc6S-L and of the heterogeneous diastereomers (lower panel) IdoA-GlcNAc6S-GlcA-GlcNAc6S-L and GlcA-GlcNAc6S-IdoA-GlcNAc6S-L. (b) Overlay of the linear combinations. Abbreviated are β-D-glucuronic acid GlcA, α-L-iduronic acid IdoA, 6-*O*-sulfo-*N*-acetyl-α-D-glucosamine GlcNAc6S and aminoalkyl-linker L ($(CH_2)_5NH_2$).

reducing end, adjacent to the aminoalkyl-linker L. In the region of the antisymmetric SO_3^- stretching modes and also around 1600 cm^{-1}, the two linear combinations reveal very similar absorption patterns, which becomes especially apparent in the overlay of the linear combinations in Figure 3b. The IR signatures between 1000 and 1150 cm^{-1} and above 1600 cm^{-1} are more congested and, even though qualitatively matching, did not line up perfectly.

To investigate the structural motifs that lead to the differences in the IR signatures, the conformational space of the four disaccharides was explored using the evolutionary algorithm FAFOOM[28] with local density functional theory optimization in FHI-aims.[29] Details on the theoretical methods are included in the Supporting Information. The sampled structures were screened for differences in the interaction between the carboxyl, amide, sulfate, and potentially present aminoalkyl-linker with relevant distances less than 2 Å. For each building block, low-energy structures with these distinct interaction motifs were reoptimized, and vibrational frequencies were computed in Gaussian 16[30] at the PBE0-D3/6-31G(d)[31,32] level of theory for all atoms except sulfur, for which the basis set 6-311+G(2df,2pd) was employed. Low-energy structures below an arbitrary threshold of 15 kJ mol^{-1} relative to the lowest-energy structure of each building block are listed with their type of interaction and their relative free energy in Table S1 (Supporting Information). The lowest-energy structure of each building block was reoptimized and the frequencies computed at PBE0-D3/ma-def2-TZVP[33,34] level of theory for all atoms.

The lowest-energy structures for the four disaccharides reveal four different structural motifs, which are depicted in Figure 4a for the nonreducing end disaccharides GlcA-GlcNAc6S and IdoA-GlcNAc6S and in Figure 4b for the disaccharides with aminoalkyl-linker GlcA-GlcNAc6S-L and IdoA-GlcNAc6S-L. The native disaccharide GlcA-GlcNAc6S predominantly forms a Type A pattern in hydrogen bonding in

https://dx.doi.org/10.1021/acs.analchem.0c02048
Anal. Chem. 2020, 92, 10228−10232

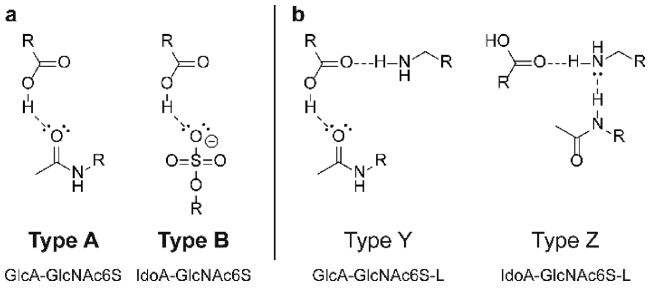

Figure 4. Structural motifs in the lowest-energy structures for (a) GlcA-GlcNAc6S (left), IdoA-GlcNAc6S (right) and (b) GlcA-GlcNAc6S-L (left), IdoA-GlcNAc6S-L (right). Abbreviated are β-D-glucuronic acid GlcA, α-L-iduronic acid IdoA, 6-*O*-sulfo-*N*-acetyl-α-D-glucosamine GlcNAc6S and aminoalkyl-linker L ($(CH_2)_5NH_2$).

which the amide carbonyl oxygen acts as hydrogen bond acceptor for the neutral carboxyl OH.

The epimer IdoA-GlcNAc6S shows preference for a Type B hydrogen bonding pattern in which the charged sulfate group forms an ionic hydrogen bond with the neutral carboxyl. The structural motif in the disaccharides with aminoalkyl-linker is dominated by an interaction between three of the functional groups in question: the amide carbonyl from GlcNAc, the neutral carboxyl group from the hexuronic acid and the amino group from the linker.

In conclusion, we show here that cryogenic IR spectroscopy is capable of unambiguously distinguishing isomeric heparan sulfate oligosaccharides that differ only in the configuration of hexuronic acid building blocks. In a wider context, the findings show that IR spectroscopy of mass-selected ions displays great potential for the analysis of heparan sulfate and heparin. Reference spectra from further small building blocks such as those reported here facilitates their identification. Cryogenic IR spectroscopy may be combined with offline chromatographic or electrophoretic separations, ion mobility spectrometry, or tandem MS techniques to significantly improve the fragment-based sequencing[17] of longer GAG chains in the future. Furthermore, our study reveals a strong spectra-structure correlation for this set of ions, which results from key intramolecular interactions that are unique for the individual stereoisomers and can be directly linked to specific structural elements. It is not clear whether these unique structural motifs are preserved in larger GAG ions, which is an interesting question for further investigations. The differences in the detailed molecular structure of the ions will help to unravel differences in the currently poorly understood fragmentation behavior of GAGs in MS experiments.

■ ASSOCIATED CONTENT

Supporting Information

The Supporting Information is available free of charge at https://pubs.acs.org/doi/10.1021/acs.analchem.0c02048.

Details on quantum chemical calculations, Cartesian coordinates of the obtained lowest-energy structures, and the investigated chemical structures in their representation in symbol nomenclature for glycans (PDF)

■ AUTHOR INFORMATION

Corresponding Author

Kevin Pagel − *Department of Molecular Physics, Fritz Haber Institute of the Max Planck Society, 14195 Berlin, Germany; Institut für Chemie und Biochemie, Freie Universität Berlin, 14195 Berlin, Germany;* orcid.org/0000-0001-8054-4718; Email: kevin.pagel@fu-berlin.de

Authors

Maike Lettow − *Department of Molecular Physics, Fritz Haber Institute of the Max Planck Society, 14195 Berlin, Germany; Institut für Chemie und Biochemie, Freie Universität Berlin, 14195 Berlin, Germany*

Márkó Grabarics − *Department of Molecular Physics, Fritz Haber Institute of the Max Planck Society, 14195 Berlin, Germany; Institut für Chemie und Biochemie, Freie Universität Berlin, 14195 Berlin, Germany;* orcid.org/0000-0002-2550-637X

Kim Greis − *Department of Molecular Physics, Fritz Haber Institute of the Max Planck Society, 14195 Berlin, Germany; Institut für Chemie und Biochemie, Freie Universität Berlin, 14195 Berlin, Germany*

Eike Mucha − *Department of Molecular Physics, Fritz Haber Institute of the Max Planck Society, 14195 Berlin, Germany*

Daniel A. Thomas − *Department of Molecular Physics, Fritz Haber Institute of the Max Planck Society, 14195 Berlin, Germany;* orcid.org/0000-0001-9415-5991

Pradeep Chopra − *Complex Carbohydrate Research Center, University of Georgia, Athens, Georgia 30602, United States;* orcid.org/0000-0002-6003-4574

Geert-Jan Boons − *Complex Carbohydrate Research Center, University of Georgia, Athens, Georgia 30602, United States; Department of Chemical Biology and Drug Discovery, Utrecht Institute for Pharmaceutical Science, and Bijvoet Center for Biomolecular Research, Utrecht University, 3584 CG Utrecht, The Netherlands;* orcid.org/0000-0003-3111-5954

Richard Karlsson − *Copenhagen Centre for Glycomics, Department of Cellular and Molecular Medicine, University of Copenhagen, Copenhagen N 2200, Denmark*

Jeremy E. Turnbull − *Copenhagen Centre for Glycomics, Department of Cellular and Molecular Medicine, University of Copenhagen, Copenhagen N 2200, Denmark; Centre for Glycobiology, Department of Biochemistry, University of Liverpool, Liverpool L69 7ZB, United Kingdom*

Gerard Meijer − *Department of Molecular Physics, Fritz Haber Institute of the Max Planck Society, 14195 Berlin, Germany;* orcid.org/0000-0001-9669-8340

Rebecca L. Miller − *Copenhagen Centre for Glycomics, Department of Cellular and Molecular Medicine, University of Copenhagen, Copenhagen N 2200, Denmark*

Gert von Helden − *Department of Molecular Physics, Fritz Haber Institute of the Max Planck Society, 14195 Berlin, Germany;* orcid.org/0000-0001-7611-8740

Complete contact information is available at: https://pubs.acs.org/10.1021/acs.analchem.0c02048

Author Contributions

§M.L. and M.G. contributed equally.

Notes

The authors declare no competing financial interest.

https://dx.doi.org/10.1021/acs.analchem.0c02048
Anal. Chem. 2020, 92, 10228−10232

■ ACKNOWLEDGMENTS

The authors gratefully acknowledge the expertise of Sandy Gewinner and Dr. Wieland Schöllkopf of the FHI FEL. K.G. thanks the Fonds National de la Recherche (FNR), Luxembourg for funding for Project GlycoCat (Grant 13549747). D.A.T. acknowledges support from the Alexander von Humboldt Foundation. This research is funded by the Deutsche Forschungsgemeinschaft (DFG, German Research Foundation) Projektnummer 372486779, SFB 1340, and the Danish National Research Foundation (Grant DNFR107).

■ REFERENCES

(1) Rabenstein, D. L. *Nat. Prod. Rep.* **2002**, *19*, 312−331.
(2) Gandhi, N. S.; Mancera, R. L. *Chem. Biol. Drug Des.* **2008**, *72* (6), 455−482.
(3) Capila, I.; Linhardt, R. J. *Angew. Chem., Int. Ed.* **2002**, *41* (3), 390−412.
(4) Soares da Costa, D.; Reis, R. L.; Pashkuleva, I. *Annu. Rev. Biomed. Eng.* **2017**, *19* (1), 1−26.
(5) Kjellén, L.; Lindahl, U. *Curr. Opin. Struct. Biol.* **2018**, *50*, 101−108.
(6) Wolff, J. J.; Leach, F. E.; Laremore, T. N.; Kaplan, D. A.; Easterling, M. L.; Linhardt, R. J.; Amster, I. J. *Anal. Chem.* **2010**, *82*, 3460−3466.
(7) Leach, F. E.; Riley, N. M.; Westphall, M. S.; Coon, J. J.; Amster, I. J. *J. Am. Soc. Mass Spectrom.* **2017**, *28* (9), 1844−1854.
(8) Huang, Y.; Yu, X.; Mao, Y.; Costello, C. E.; Zaia, J.; Lin, C. *Anal. Chem.* **2013**, *85*, 11979−11986.
(9) Alocci, D.; Ghraichy, M.; Barletta, E.; Gastaldello, A.; Mariethoz, J.; Lisacek, F. *Glycobiology* **2018**, *28* (6), 349−362.
(10) Wolff, J. J.; Chi, L.; Linhardt, R. J.; Amster, I. J. *Anal. Chem.* **2007**, *79*, 2015−2022.
(11) Oh, H. B.; Leach, F. E.; Arungundram, S.; Al-Mafraji, K.; Venot, A.; Boons, G.-J.; Amster, I. J. *J. Am. Soc. Mass Spectrom.* **2011**, *22* (3), 582−590.
(12) Agyekum, I.; Zong, C.; Boons, G.-J.; Amster, I. J. *J. Am. Soc. Mass Spectrom.* **2017**, *28* (9), 1741−1750.
(13) Wu, J.; Wei, J.; Chopra, P.; Boons, G.-J.; Lin, C.; Zaia, J. *Anal. Chem.* **2019**, *91* (18), 11738−11746.
(14) Kailemia, M. J.; Park, M.; Kaplan, D. A.; Venot, A.; Boons, G.-J.; Li, L.; Linhardt, R. J.; Amster, I. J. *J. Am. Soc. Mass Spectrom.* **2014**, *25*, 258−268.
(15) Miller, R. L.; Wei, W.; Schwörer, R.; Zubkova, O. V.; Tyler, P. C.; Turnbull, J. E.; Leary, J. A. *Eur. J. Mass Spectrom.* **2015**, *21* (3), 245−254.
(16) Wei, J.; Wu, J.; Tang, Y.; Ridgeway, M. E.; Park, M. A.; Costello, C. E.; Zaia, J.; Lin, C. *Anal. Chem.* **2019**, *91* (4), 2994−3001.
(17) Miller, R. L.; Guimond, S. E.; Schwörer, R.; Zubkova, O. V.; Tyler, P. C.; Xu, Y.; Liu, J.; Chopra, P.; Boons, G.-J.; Grabarics, M.; Manz, C.; Hofmann, J.; Karlsson, N. G.; Turnbull, J. E.; Struwe, W. B.; Pagel, K. *Nat. Commun.* **2020**, *11* (1), 1481.
(18) Lettow, M.; Grabarics, M.; Mucha, E.; Thomas, D. A.; Polewski, Ł.; Freyse, J.; Rademann, J.; Meijer, G.; von Helden, G.; Pagel, K. *Anal. Bioanal. Chem.* **2020**, *412* (3), 533−537.
(19) Schindler, B.; Barnes, L.; Gray, C. J.; Chambert, S.; Flitsch, S. L.; Oomens, J.; Daniel, R.; Allouche, A. R.; Compagnon, I. *J. Phys. Chem. A* **2017**, *121* (10), 2114−2120.
(20) Khanal, N.; Masellis, C.; Kamrath, M. Z.; Clemmer, D. E.; Rizzo, T. R. *Anal. Chem.* **2017**, *89* (14), 7601−7606.
(21) Compagnon, I.; Schindler, B.; Renois-Predelus, G.; Daniel, R. *Curr. Opin. Struct. Biol.* **2018**, *50*, 171−180.
(22) Schindler, B.; Renois-Predelus, G.; Bagdadi, N.; Melizi, S.; Barnes, L.; Chambert, S.; Allouche, A.-R.; Compagnon, I. *Glycoconjugate J.* **2017**, *34* (3), 421−425.
(23) Thomas, D. A.; Marianski, M.; Mucha, E.; Meijer, G.; Johnson, M. A.; von Helden, G. *Angew. Chem., Int. Ed.* **2018**, *57* (33), 10615−10619.
(24) Gonzalez Florez, A. I.; Ahn, D. S.; Gewinner, S.; Schollkopf, W.; von Helden, G. *Phys. Chem. Chem. Phys.* **2015**, *17* (34), 21902−11.
(25) Thomas, D. A.; Mucha, E.; Lettow, M.; Meijer, G.; Rossi, M.; von Helden, G. *J. Am. Chem. Soc.* **2019**, *141* (14), 5815−5823.
(26) Arungundram, S.; Al-Mafraji, K.; Asong, J.; Leach, F. E.; Amster, I. J.; Venot, A.; Turnbull, J. E.; Boons, G.-J. *J. Am. Chem. Soc.* **2009**, *131* (47), 17394−17405.
(27) Struwe, W. B.; Baldauf, C.; Hofmann, J.; Rudd, P. M.; Pagel, K. *Chem. Commun.* **2016**, *52* (83), 12353−12356.
(28) Supady, A.; Blum, V.; Baldauf, C. *J. Chem. Inf. Model.* **2015**, *55* (11), 2338−48.
(29) Blum, V.; Gehrke, R.; Hanke, F.; Havu, P.; Havu, V.; Ren, X.; Reuter, K.; Scheffler, M. *Comput. Phys. Commun.* **2009**, *180* (11), 2175−2196.
(30) Frisch, M. J.; Trucks, G. W.; Schlegel, H. B.; Scuseria, G. E.; Robb, M. A.; Cheeseman, J. R.; Scalmani, G.; Barone, V.; Petersson, G. A.; Nakatsuji, H.; Li, X.; Caricato, M.; Marenich, A. V.; Bloino, J.; Janesko, B. G.; Gomperts, R.; Mennucci, B.; Hratchian, H. P.; Ortiz, J. V.; Izmaylov, A. F.; Sonnenberg, J. L.; Williams; Ding, F.; Lipparini, F.; Egidi, F.; Goings, J.; Peng, B.; Petrone, A.; Henderson, T.; Ranasinghe, D.; Zakrzewski, V. G.; Gao, J.; Rega, N.; Zheng, G.; Liang, W.; Hada, M.; Ehara, M.; Toyota, K.; Fukuda, R.; Hasegawa, J.; Ishida, M.; Nakajima, T.; Honda, Y.; Kitao, O.; Nakai, H.; Vreven, T.; Throssell, K.; Montgomery, J. A., Jr.; Peralta, J. E.; Ogliaro, F.; Bearpark, M. J.; Heyd, J. J.; Brothers, E. N.; Kudin, K. N.; Staroverov, V. N.; Keith, T. A.; Kobayashi, R.; Normand, J.; Raghavachari, K.; Rendell, A. P.; Burant, J. C.; Iyengar, S. S.; Tomasi, J.; Cossi, M.; Millam, J. M.; Klene, M.; Adamo, C.; Cammi, R.; Ochterski, J. W.; Martin, R. L.; Morokuma, K.; Farkas, O.; Foresman, J. B.; Fox, D. J. *Gaussian 16*, rev. A.03; Guassian Inc.: Wallingford, CT, 2016.
(31) Adamo, C.; Barone, V. *J. Chem. Phys.* **1999**, *110* (13), 6158−6170.
(32) Grimme, S.; Antony, J.; Ehrlich, S.; Krieg, H. *J. Chem. Phys.* **2010**, *132* (15), 154104.
(33) Weigend, F.; Ahlrichs, R. *Phys. Chem. Chem. Phys.* **2005**, *7* (18), 3297−3305.
(34) Zheng, J.; Xu, X.; Truhlar, D. G. *Theor. Chem. Acc.* **2011**, *128* (3), 295−305.

https://dx.doi.org/10.1021/acs.analchem.0c02048
Anal. Chem. 2020, 92, 10228−10232